(Received 30 October 2025, Accepted 11 November 2025, Scheduled 19 December 2025)

Broadband Validation of a 2D-FDTD-PML and Nelder-Mead Framework for Liquid Permittivity Extraction

Omaima Talmoudi[1,*], Lahcen Ait Benali[2], Jaouad Terhzaz[2], and Abdelwahed Tribak[1]

[1] *Institut National des Postes et Télécommunications (INPT), Rabat, Morocco*
[2] *CRMEF Casablanca-Settat, Casablanca, Morocco*

ABSTRACT: A methodology for estimating the complex permittivity of liquid dielectrics is presented in a rectangular waveguide using the Ku-band (10–15 GHz, WR75). A two-dimensional finite difference time-domain (FDTD) model with perfectly matched layers (PMLs) serves as the forward solver, and TE_{10} modal projection provides the simulated scattering parameters. Subsequently, a gradient-free Nelder-Mead inversion extracts the real and imaginary parts of the permittivity from the measured S_{11} and S_{21} parameters. This approach is implemented in a multilayer fixture, which enables leak-tight loading while remaining analytically simple. Validation on air and water shows good agreement between simulation and measurement across 10–15 GHz, and results at 12 GHz are consistent with independent X-band extractions. This approach is computationally efficient, practical for experimentation, and can be extended to other liquids and multilayers.

1. INTRODUCTION

Accurately determining the complex permittivity of dielectric materials, including both the real and imaginary components, is a fundamental requirement in many areas of science and engineering [1, 2]. Liquid dielectrics present unique characterization challenges due to their temperature sensitivity, potential for container effects, and the necessity of non-destructive measurement techniques. Reliable permittivity data are essential for designing and optimizing devices and systems in diverse fields, such as microwave sensing, wireless communication, geophysical surveying, biomedical diagnostics, and industrial quality control [3–6]. In the microwave frequency range, rectangular waveguide measurement techniques are widely recognized for their precision and repeatability. These techniques offer a well-defined modal structure and strong compatibility with standard calibration procedures for vector network analyzers [7, 8].

Several strategies have been developed to extract the permittivity of materials positioned within a waveguide. Analytical models, derived from transmission-line or modal analysis theory, provide closed-form expressions linking measured scattering parameters to the dielectric properties [9, 10]. For instance, established techniques such as the two-port transmission line method proposed [11, 12]. Use dielectric plugs to contain liquid or granular samples and rely on these analytical formulations for direct permittivity calculation. These models are computationally efficient. However, they may neglect higher-order mode interactions and discontinuities. In contrast, full-wave numerical techniques, such as the finite-difference time-domain (FDTD) and finite element method (FEM), possess the capacity to accurately account for complex geometries, dispersive behavior, and loss mechanisms [13, 14].

Recent studies have highlighted that hybrid strategies, which combine analytical and numerical modeling, improve efficiency, particularly when supported by robust optimization algorithms. Gradient-free techniques, including the Nelder-Mead simplex, are effective for retrieving complex permittivity under noisy conditions [15, 16].

Building upon our previous validation in the X-band [7], this work presents three key contributions. First, it shows that the hybrid framework operates consistently in the Ku band, indicating that the method behaves robustly and reliably across different frequency ranges. Second, operating at a higher frequency establishes the utility of the technique for applications demanding greater sensitivity to dielectric variations, such as high-resolution sensing. Third, it details the implementation and validation of a multilayer test fixture tailored for the Ku-band, which addresses the practical challenges of characterizing liquids at these frequencies. This extension is a crucial step in establishing the proposed framework as a widely applicable tool for extracting liquid permittivity.

2. THEORY

2.1. Geometry, Assumptions, and Notation

In this study, a standard rectangular WR75 waveguide, characterized by a cross-section of dimensions $a \times b$, is excited in the dominant TE_{10} mode. A three-layer dielectric stack is inserted along the longitudinal axis z: a front resin plug of thickness d_1, the liquid under test of thickness d_2, and a back resin plug of thickness d_1 as shown in Fig. 1. The complex relative permittivities are denoted as ε_{r1} for resin and ε_r for the unknown material. The reference planes for the S-parameters are located at $z = d_1$ and $z = 2d_1 + d_2$.

* Corresponding author: Omaima Talmoudi (omaimatalmoudi@gmail.com).

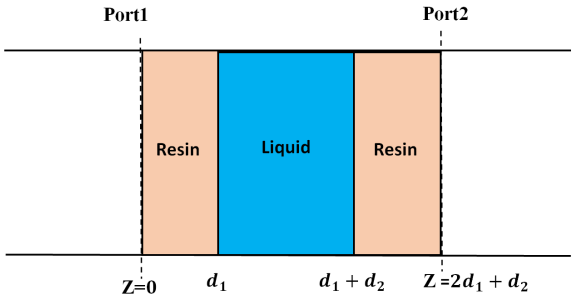

FIGURE 1. Rectangular waveguide loaded with a multilayer dielectric material.

2.2. Numerical Forward Model: 2D FDTD with PML

In the numerical approach, electromagnetic wave propagation is modeled using the two-dimensional finite-difference time-domain (FDTD) method and perfectly matched layer (PML) absorbing boundaries.

For the dominant TE_{10} mode, the transverse electric field component E_y satisfies the wave equation:

$$\frac{\partial^2 E_y}{\partial t^2} = \frac{1}{\varepsilon_r \mu_r}\left(\frac{\partial^2 E_y}{\partial x^2} + \frac{\partial^2 E_y}{\partial z^2}\right), \tag{1}$$

where ε_r and μ_r denote the relative permittivity and permeability of the medium, respectively.

Using Yee's notation [16], the FDTD formulation of E_y in Cartesian coordinates is obtained by applying second-order central differences in time and space, yielding:

$$\begin{aligned} E_{i,k}^{n+1} &= 2E_{i,k}^{n} - E_{i,k}^{n-1} \\ &+ \frac{c^2\Delta t^2}{\varepsilon_r(i,k)}\left(\frac{E_{i+1,k}^{n} + E_{i-1,k}^{n} - 2E_{i,k}^{n}}{\Delta x^2}\right. \\ &\left. + \frac{E_{i,k+1}^{n} + E_{i,k-1}^{n} - 2E_{i,k}^{n}}{\Delta z^2}\right), \end{aligned} \tag{2}$$

where (i,k) denotes the spatial grid indices, and n denotes the time step. This formulation relates the field at the time step $n+1$ to its present and past values, as well as to the spatial variations in both x- and z-directions. Equation (2) serves as the basis of the forward FDTD simulation with PML boundaries. In the two-dimensional FDTD discretization, Δx and Δz represent the spatial steps along the x- and z-direction, while Δt denotes the time step. For sufficient accuracy, the mesh size must be small compared to the guided wavelength:

$$\max(\Delta x, \Delta z) < \frac{\lambda_g}{m_0}, \tag{3}$$

where λ_g is the guided wavelength, and m_0 is a discretization factor typically chosen in the range $10 < m_0 < 100$.

To achieve numerical stability of the 2D-FDTD algorithm, the time step Δt and spatial increments Δx and Δz must respect the following stability condition [13]:

$$\Delta t \leq \frac{1}{c}\frac{1}{\sqrt{\Delta x^{-2} + \Delta z^{-2}}}, \tag{4}$$

where c is the speed of light in free space.

2.2.1. PML Boundary Truncation

To prevent spurious reflections at the computational boundaries, perfectly matched layer (PML) absorbing regions are applied at the extremities of the z-axis. In the auxiliary differential equation (ADE) approach, the field update equations are modified within the PML to include an electric conductivity profile σ_z and a scaling factor κ_z that attenuates outgoing waves.

At the lower boundary ($z = 0$):

$$\begin{aligned} &E^{n+1}(i,0) \\ &= \frac{2-\sigma_z(0)\Delta t}{2+\sigma_z(0)\Delta t}\left[2E^{n}(i,0) - E^{n-1}(i,0)\right] \\ &+ \frac{c^2\Delta t^2}{\varepsilon_r(i,0)}\left[\frac{E^{n}(i+1,0) + E^{n}(i-1,0) - 2E^{n}(i,0)}{\Delta x^2}\right. \\ &\left. + \frac{1}{\kappa_z^2(0)}\frac{E^{n}(i,1) - E^{n}(i,0)}{\Delta z^2}\right] \end{aligned} \tag{5}$$

At the upper boundary ($z = z_{\max}$):

$$E^{n+1}(i, z_{\max}) \tag{6}$$

$$\begin{aligned} &= \frac{2-\sigma_z(z_{\max})\Delta t}{2+\sigma_z(z_{\max})\Delta t}\left[2E^{n}(i,z_{\max}) - E^{n-1}(i,z_{\max})\right] \\ &+ \frac{c^2\Delta t^2}{\varepsilon_r(i,z_{\max})} \end{aligned} \tag{7}$$

$$\begin{aligned} &\left[\frac{E^{n}(i+1,z_{\max}) + E^{n}(i-1,z_{\max}) - 2E^{n}(i,z_{\max})}{\Delta x^2}\right. \\ &\left. + \frac{1}{\kappa_z^2(z_{\max})}\frac{E^{n}(i,z_{\max}-1) - E^{n}(i,z_{\max})}{\Delta z^2}\right] \end{aligned} \tag{8}$$

2.2.2. Excitation and Modal Sampling

The waveguide is excited by a TE_{10} mode source located at $z = z_{\text{src}}$. The temporal excitation is a Gaussian-modulated sinusoid, ensuring a central frequency ω_0 and a controlled spectral width determined by τ. The spatial dependence along x matches the fundamental mode profile of the rectangular waveguide:

$$E(i,k_{\text{src}}) = \exp\left[-\frac{(t-t_0)^2}{\tau^2}\right]\sin(\omega_0 t)\,\sin\left(\frac{\pi i \Delta x}{a}\right), \tag{9}$$

where a is the waveguide width.

After reaching steady state, the field distribution is projected onto the TE_{10} mode to extract the forward and backward wave amplitudes. This projection is performed at two adjacent planes z_1 and $z_1 + \Delta z$ near the input, and at a plane z_3 near the output:

$$m_1 = \int_0^a E(x,z_1)\sin\frac{\pi x}{a}\,dx = A(z_1) + B(z_1) \tag{10}$$

$$m_2 = \int_0^a E(x,z_1+\Delta z)\sin\frac{\pi x}{a}dx = Ae^{-j\gamma\Delta z} + Be^{+j\gamma\Delta z} \tag{11}$$

$$m_3 = \int_0^a E(x, z_3) \sin\frac{\pi x}{a}\, dx = A(z_3) \tag{12}$$

Here, $\sin(\frac{\pi x}{a})$ represents the normalized modal magnetic field, and $\gamma = \sqrt{(\frac{\omega}{c})^2 - (\frac{\pi}{a})^2}$ is the modal propagation constant. This results in the following expressions:

$$S_{11} = \frac{m_2 - m_1 e^{-j\gamma\Delta z}}{m_1 e^{+j\gamma\Delta z} - m_2} \tag{13}$$

$$S_{21} = \frac{m_3\left(e^{+j\gamma\Delta z} - e^{-j\gamma\Delta z}\right)}{m_1 e^{+j\gamma\Delta z} - m_2} \tag{14}$$

2.3. Inverse Problem

This section outlines the procedure used to estimate the complex permittivity of the liquid dielectric under study. The liquid is confined within a layer of known thickness, sealed between two resin samples positioned at the ends of a rectangular waveguide to ensure tightness. The estimation process relies on the `Fmin` function in Python [17], which applies the Nelder-Mead simplex algorithm [18]. This algorithm is well-suited for solving nonlinear, unconstrained, multivariable optimization problems. The optimization begins from an initial guess for the complex relative permittivity, for example $\varepsilon_r' = 1.5$ and $\varepsilon_r'' = 0.005\varepsilon_r'$, with a convergence tolerance of 10^{-3} and a limit of 100 iterations. The goal is to minimize an error function defined as the sum of squared differences between the measured and simulated scattering parameters S_{ij}, as expressed in the following equation [7].

$$f(\varepsilon_r', \varepsilon_r'') = \sum \|S_{ijcal} - S_{ijmeas}\|^2 \tag{15}$$

3. NUMERICAL RESULTS

A vector network analyzer (VNA) was employed to measure the scattering parameters,S_{11} and S_{21} of a modified WR75 rectangular waveguide fixture for Ku-band measurements (10–15 GHz). Before measurement, the VNA was calibrated to the WR75 reference planes.

To confine the liquid under test, a solid dielectric plug was mounted in the transverse plane, providing a leak-tight seal and isolating the measurement section. A small aperture along the longitudinal axis functioned as a fill port, enabling controlled liquid injection into the test region as illustrated in Fig. 2. This configuration minimized leakage and handling errors, stabilized the sample volume, and improved measurement repeatability, thereby enhancing the reliability of the extracted dielectric properties.

3.1. Direct Problem

3.1.1. Convergence

To verify the robustness and accuracy of the numerical scheme, a convergence study was first performed for an empty Ku-band rectangular waveguide of length $L = 10\,\text{mm}$. The simulation employed discretization steps of $\Delta x = 0.75\,\text{mm}$, $\Delta z = 0.08\,\text{mm}$, and a time step of $\Delta t = 0.265\,\text{ps}$, with a total of 5000 iterations.

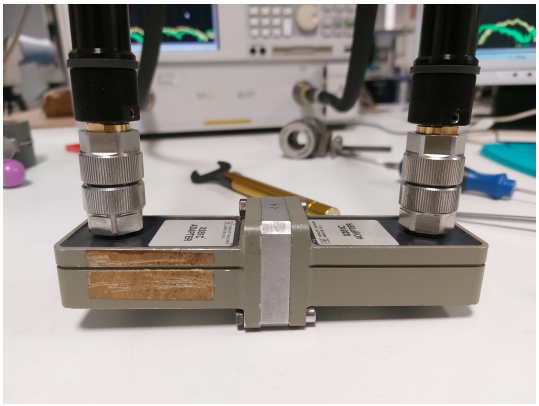

FIGURE 2. Measurement system for Ku-band waveguide characterization.

The convergence curve presented in Fig. 3 demonstrated stable numerical behavior and reliable field evolution over time, confirming proper implementation of the FDTD-PML algorithm. This demonstrates the ability of the method to accurately resolve the electromagnetic response of the Ku-band waveguide.

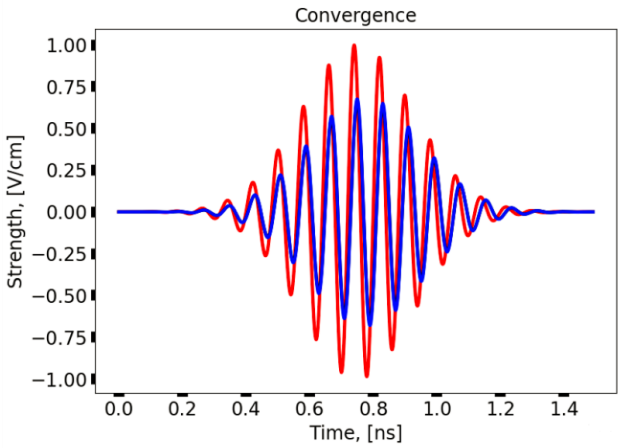

FIGURE 3. Convergence behavior of the Ku-band FDTD-PML numerical model.

The observation of stable convergence ensures that the approach can be applied with confidence for subsequent dielectric characterization and S-parameter extraction. Furthermore, analyzing the electric field signals (at the excitation plane and after sample traversal) revealed that both signals decayed to zero, confirming simulation stability. The amplitude difference and time delay observed between these signals correspond directly to the dielectric loss and wave propagation time of the material.

3.1.2. Characterization of an Empty Rectangular Waveguide

After confirming convergence, the direct problem was examined by computing the S-parameters of a Ku-band rectangular

waveguide filled with air ($\varepsilon_r' = 1$, $\varepsilon_r'' = 0$) as a baseline check to confirm the FDTD model correctly accounts for the resin plugs and fixture geometry before testing with liquids. The simulated results were compared against experimental measurements performed in the Ku-band.

As illustrated in Fig. 4, the results exhibit low reflection (S_{11}) and stable transmission (S_{21}), confirming efficient propagation through the empty waveguide. The observed agreement between the FDTD-PML predictions and the measured data is consistent with the expected performance of the proposed numerical model in the Ku band.

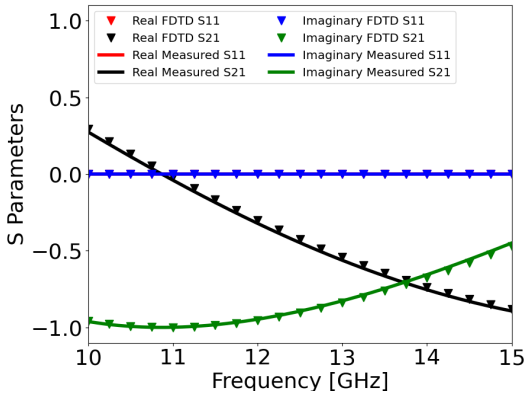

FIGURE 4. S_{11} and S_{21} parameters of an empty Ku-band rectangular waveguide.

3.1.3. Analysis of a Rectangular Waveguide with Resin Walls and Empty Interior

The next stage of the direct problem focused on evaluating a Ku-band rectangular waveguide modified to include a small aperture for liquid injection. The electromagnetic response of this structure was analyzed using the 2D FDTD-PML method and compared with Ku-band measurements to evaluate the performance of the numerical approach

The configuration incorporated resin walls of thickness 3 mm, characterized by a complex permittivity of $\varepsilon_r' = 3.2$ and $\varepsilon_r'' = 0.02$. The walls were positioned directly at the ports, effectively enclosing the test region while maintaining the possibility of liquid insertion through the side opening, as illustrated in Fig. 5.

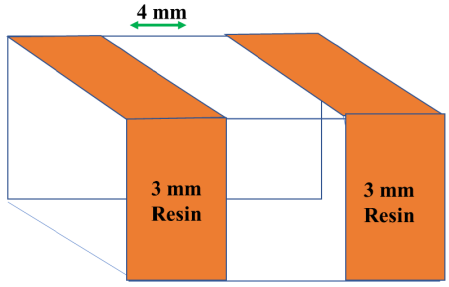

FIGURE 5. Ku-band rectangular waveguide with 3 mm resin walls and an empty interior.

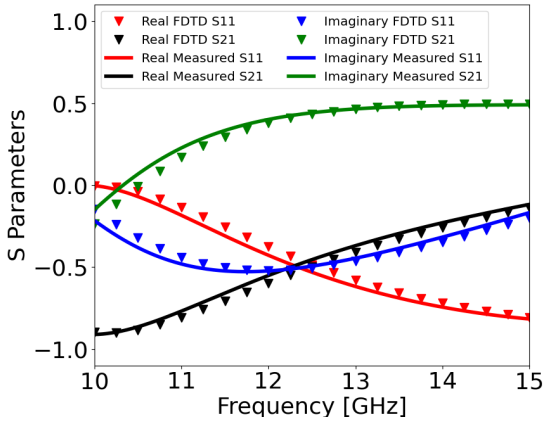

FIGURE 6. S_{11} and S_{21} parameters of a Ku-band rectangular waveguide enclosed with resin walls and an empty interior.

As presented in Fig. 6, the simulated and measured S_{11} and S_{21} parameters show close agreement across the Ku-band frequency range. These results demonstrate that the FDTD-PML formulation accurately models the electromagnetic behavior of multilayer Ku-band structures, including dielectric losses and dispersion. This confirms the suitability of the proposed method for characterizing more complex material configurations.

3.2. Inverse Problem

3.2.1. Estimation of Air Complex Permittivity in a Resin-Loaded Rectangular Waveguide

For initial validation purposes, the rectangular waveguide was closed with resin walls ($\varepsilon_r' = 3.2$, $\varepsilon_r'' = 0.02$) and the central section was filled with air. As the exact dielectric properties of air were not assumed a priori, the inversion procedure was initialised using an arbitrary guess ($\varepsilon_r' = 1.5$, $\varepsilon_r'' = 0.005$). The 2D FDTD-PML solver was then used to calculate the scattering parameters, which were iteratively matched to the measured data using the Nelder-Mead simplex algorithm.

The results obtained in Fig. 7 confirm the expected dielectric behavior of air, with a real part close to 1 and an imaginary part of approximately 10^{-3}. This supports the suitability of the proposed inversion method to accurately recover the properties of low-loss media, even in the presence of resin walls.

3.2.2. Estimation of Water Complex Permittivity in a Resin-Loaded Rectangular Waveguide

In the second test, the Ku-band waveguide structure was filled with water while the resin walls were left in place. Initialisation of the inversion again started from a generic permittivity point, and the FDTD-PML model was coupled with Nelder-Mead optimization to minimise the error between the measured and simulated scattering parameters.

As expected, the extracted results presented in Fig. 8 show the dispersive behavior of liquid water in the Ku-band: the real part of the permittivity decreases from approximately 62.5 at 10 GHz to about 48.5 at 15 GHz, while the imaginary part increases from roughly 34 to 38.5 over the same range.

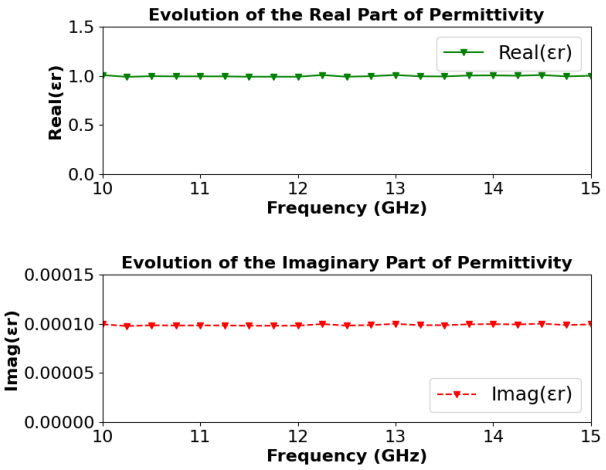

FIGURE 7. Extracted real and imaginary parts of the relative permittivity of air inside a Ku-band rectangular waveguide sealed with resin walls.

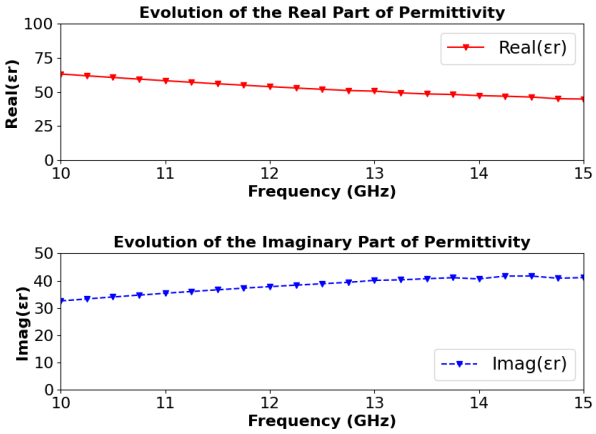

FIGURE 8. Extracted real and imaginary parts of the relative permittivity of distilled water inside a Ku-band rectangular waveguide sealed with resin walls.

The measurement uncertainty analysis quantified the stability of the extracted complex permittivity, accounting for the primary sources of variation. The accuracy of the vector network analyzer (VNA) instrument, the dimensional tolerance of the WR75 waveguide (± 0.02 mm), the thickness precision of the liquid sample (± 0.01 mm), and the residual errors after TRL calibration were all evaluated. Each contribution was propagated through the extraction procedure and combined using the root-sum-square (RSS) method. The expanded uncertainty was obtained with a coverage factor $k = 2$, corresponding to a 95% confidence level. The resulting expanded relative uncertainties are approximately $\pm 4.1\%$ for the real part (ε') and $\pm 4.0\%$ for the imaginary part (ε'') of the permittivity. These figures demonstrate that the observed deviations across frequency bands lie well within the expected experimental limits, confirming the stability and validity of the presented framework.

Before analyzing the agreement between the different frequency bands, this work focuses on the Ku-band results, as they rely on the most complete formulation of the hybrid 2D FDTD-PML and Nelder-Mead inversion scheme. To quantify the consistency of the permittivity values across datasets, the complex permittivity reported by [19] and our previously published X-band measurements [7] were directly compared to the Ku-band result at 12 GHz.

As shown in Table 1, the X-band results exhibit very small deviations from the Ku-band reference, with relative differences of 1.14% for the real part and 1.08% for the imaginary part. These values fall well within typical measurement uncertainties and confirm the robustness of the experimental protocol used in our earlier work. The comparison with the canonical Ellison model also shows good agreement, with deviations of approximately 2.18% for both ε' and ε''.

This level of consistency across independent references indicates that the proposed hybrid inversion method provides stable results for dielectric characterization using rectangular waveguides.

TABLE 1. Comparison of the complex permittivity obtained at 12 GHz.

Band (12 GHz)	ε'	ε''	$\Delta\varepsilon'$ (%)	$\Delta\varepsilon''$ (%)
Reference [19]	55.40	35.80	2.18	2.18
X-band [7]	56.00	37.00	1.14	1.08
Ku-band (this work, reference)	56.64	36.60	-	-

4. CONCLUSION

In this study, a hybrid framework combining 2D-FDTD-PML modeling and Nelder Mead inversion has demonstrated reliable behaviour for liquid permittivity extraction in rectangular waveguides. Following the initial demonstration of feasibility in the X-band, the method has been extended to the Ku-band through the implementation of a multilayer sealing fixture. The extracted complex permittivity values for air and distilled water show stable behavior and strong agreement between simulation and measurement over the 10–15 GHz range, with excellent consistency observed at 12 GHz relative to independent X-band results. These findings confirm that the FDTD-PML formulation is reliable across both frequency bands and highlight the adaptability of the inversion scheme. The proposed approach can be readily generalized to other liquids, multilayer stacks, and alternative frequency bands by adjusting the fixture parameters and incorporating frequency-dependent models. The robustness and versatility of the framework make it a promising tool for characterizing liquid dielectrics in future microwave and millimeter-wave applications.

REFERENCES

[1] Krupka, J., "Microwave measurements of electromagnetic properties of materials," *Materials*, Vol. 14, No. 17, 5097, 2021.

[2] Tao, Y., B. Yan, D. Fan, N. Zhang, S. Ma, L. Wang, Y. Wu, M. Wang, J. Zhao, and H. Zhang, "Structural changes of starch subjected to microwave heating: A review from the perspective of dielectric properties," *Trends in Food Science & Technology*, Vol. 99, 593–607, 2020.

[3] Pakkathillam, J. K., B. T. Sivaprakasam, J. Poojali, C. V. Krishnamurthy, and K. Arunachalam, "Tailoring antenna focal plane characteristics for a compact free-space microwave complex dielectric permittivity measurement setup," *IEEE Transactions on Instrumentation and Measurement*, Vol. 70, 1–12, 2021.

[4] Ebara, H., T. Inoue, and O. Hashimoto, "Measurement method of complex permittivity and permeability for a powdered material using a waveguide in microwave band," *Science and Technology of Advanced Materials*, Vol. 7, No. 1, 77, 2006.

[5] Saad-Falcon, A., Z. Zhang, D. Ryoo, J. Dee, R. S. Westafer, and J. C. Gumbart, "Extraction of dielectric permittivity from atomistic molecular dynamics simulations and microwave measurements," *The Journal of Physical Chemistry B*, Vol. 126, No. 40, 8021–8029, 2022.

[6] Ma, J., J. Tang, K. Wang, L. Guo, Y. Gong, and S. Wang, "Complex permittivity characterization of liquid samples based on a split ring resonator (SRR)," *Sensors*, Vol. 21, No. 10, 3385, 2021.

[7] Talmoudi, O., L. A. Benali, J. Terhzaz, A. Tribak, and T. Fernández-Ibáñez, "A novel hybrid 2D-FDTD-PML and Nelder–Mead methods for estimating liquid complex permittivity using a rectangular waveguide," *Journal of Applied Physics*, Vol. 137, No. 14, 144501, 2025.

[8] Talmoudi, O., □. Gómez-Gómez, O. Fernandez, J. Terhzaz, A. Tribak, and T. Fernández-Ibáñez, "Substrate integrated waveguide resonator sensor for X-band dielectric constant characterization," *Journal of Applied Physics*, Vol. 138, No. 7, 074503, 2025.

[9] Hasar, U. C. and A. Cansiz, "Simultaneous complex permittivity and thickness evaluation of liquid materials from scattering parameter measurements," *Microwave and Optical Technology Letters*, Vol. 52, No. 1, 75–78, 2010.

[10] Hasar, U. C., "Permittivity measurement of thin dielectric materials from reflection-only measurements using one-port vector network analyzers," *Progress In Electromagnetics Research*, Vol. 95, 365–380, 2009.

[11] Bois, K. J., L. F. Handjojo, A. D. Benally, K. Mubarak, and R. Zoughi, "Dielectric plug-loaded two-port transmission line measurement technique for dielectric property characterization of granular and liquid materials," *IEEE Transactions on Instrumentation and Measurement*, Vol. 48, No. 6, 1141–1148, 1999.

[12] Bois, K., A. Benally, and R. Zoughi, "Two-port network analyzer dielectric constant measurement of granular or liquid materials for the study of cement based materials," in *Nondestructive Characterization of Materials VIII*, 291–296, R. E. Green (ed.), Springer, 1998.

[13] Terhzaz, J., H. Ammor, A. Assir, and A. Mamouni, "Application of the FDTD method to determine complex permittivity of dielectric materials at microwave frequencies using a rectangular waveguide," *Microwave and Optical Technology Letters*, Vol. 49, No. 8, 1964–1968, 2007.

[14] Krupezevic, D. V., V. J. Brankovic, and F. Arndt, "The wave-equation FD-TD method for the efficient eigenvalue analysis and S-matrix computation of waveguide structures," *IEEE Transactions on Microwave Theory and Techniques*, Vol. 41, No. 12, 2109–2115, 1993.

[15] Mosavirik, T., V. Nayyeri, M. Hashemi, M. Soleimani, and O. M. Ramahi, "Direct permittivity reconstruction from power measurements using a machine learning aided method," *IEEE Transactions on Microwave Theory and Techniques*, Vol. 71, No. 10, 4437–4448, 2023.

[16] Qin, J., Z. Liu, M. Ma, and Y. Li, "Machine learning approaches for permittivity prediction and rational design of microwave dielectric ceramics," *Journal of Materiomics*, Vol. 7, No. 6, 1284–1293, 2021.

[17] Python Software Foundation, "Python optimization user's guide," 2022.

[18] Nelder, J. A. and R. Mead, "A simplex method for function minimization," *The Computer Journal*, Vol. 7, No. 4, 308–313, 1965.

[19] Ellison, W. J., "Permittivity of pure water, at standard atmospheric pressure, over the frequency range-25 THz and the temperature range-100 C," *Journal of Physical and Chemical Reference Data*, Vol. 36, No. 1, 1–18, 2007.